

Cytotoxicity Study of Gold Nanoparticle Synthesis Using *Aloe vera*, Honey, and *Gymnema sylvestre* Leaf Extract

Shiza Malik, Maha Niazi, Maham Khan, Bisma Rauff, Sidra Anwar, Faheem Amin,* and Rumeza Hanif*

Cite This: *ACS Omega* 2023, 8, 6325–6336

Read Online

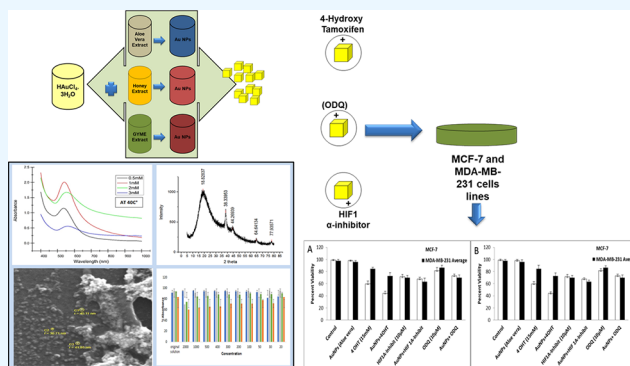
ACCESS |

Metrics & More

Article Recommendations

Supporting Information

ABSTRACT: Gold nanoparticles (AuNPs) have gained importance in the field of biomedical research and diagnostics due to their unique physicochemical properties. This study aimed to synthesize AuNPs using *Aloe vera* extract, honey, and *Gymnema sylvestre* leaf extract. Physicochemical parameters for the optimal synthesis of AuNPs were determined using 0.5, 1, 2, and 3 mM of gold salt at varying temperatures from 20 to 50 °C. X-ray diffraction was used to evaluate the crystal structure of AuNPs, which came out to be a face-centered cubic structure. Scanning electron microscopy and energy-dispersive X-ray spectroscopy analysis confirmed the size and shape of AuNPs between 20 and 50 nm from the *Aloe vera*, honey, and *Gymnema sylvestre*, as well as large-sized nanocubes in the case of honey, with 21–34 wt % of gold content. Furthermore, Fourier transform infrared spectroscopy confirmed the presence of a broadband of amine (N–H) and alcohol groups (O–H) on the surface of the synthesized AuNPs that prevents them from agglomeration and provides stability. Broad and weak bands of aliphatic ether (C–O), alkane (C–H), and other functional groups were also found on these AuNPs. DPPH antioxidant activity assay showed a high free radical scavenging potential. The most suited source was selected for further conjugation with three anticancer drugs including 4-hydroxy Tamoxifen, HIF1 α -inhibitor, and the soluble Guanylyl Cyclase Inhibitor 1 H-[1,2,4] oxadiazolo [4,3- α]quinoxalin-1-one (ODQ). Evidence of the pegylated drug conjugation with AuNPs was reinforced by ultraviolet/visible spectroscopy. These drug-conjugated nanoparticles were further checked on MCF7 and MDA-MB-231 cells for their cytotoxicity. These AuNP-conjugated drugs can be a good candidate for breast cancer treatment that will lead toward safe, economical, biocompatible, and targeted drug delivery systems.



1. INTRODUCTION

Gold nanoparticles (AuNPs) are promising candidates for biomedical applications due to their unique physicochemical properties.¹ Their applications include optics for medical diagnosis,² radiosensitizing, photothermal, and antioxidant properties for therapeutics,³ targeted drug/gene delivery, catalysis, sensing,^{4–6} and electronic conductance among others.⁷ AuNPs as drug delivery vehicles can target specific cells⁵ due to their easy surface modification,^{6–8} biocompatibility,⁹ and quenching efficiencies.^{10,11} Various AuNP-based chemotherapeutic drugs such as Aurimune (CYT-6091),¹² DNA-conjugated silver nanoclusters (DNA-AgNCs), carbon nanotube³ (La(OH)₃-OxMWCNT) nanocomposites, copper nanoparticles (poly T30-Cu NPs), auroshell,¹⁶ nanoemulsions, dendrimers, to count a few, are being progressively employed as treatment strategies.^{13–17}

Chemical methods are more frequently used for the synthesis of AuNPs.¹⁸ However, shortcomings of this approach are the use of compounds such as ethylene glycol, ascorbic acid, and NaBH₄, which result in the production of toxic residues during the synthesis and functionalization of nanoparticles (NPs). These toxic residues can be harmful to human health through

the food chain and ecosystem contamination.¹⁹ Therefore, during the last couple of decades, biological methods have gained considerable interest in the synthesis of various types of NPs.^{20–22} Biological methods using microorganisms, organic compounds, insects and their products, and most popularly plant extracts have been explored due to their ability to reduce chloroauric acid (HAuCl₄).²³ These methods are eco-friendly, cost-effective, and biologically compatible.²⁴ Chandran et al. used *Aloe vera* extract to produce gold nanotriangles. The authors attributed the formation of nanotriangles to the slow reduction of gold ions and shape-directing carbonyls in the extract.²⁵ Talib et al. prepared the *Aloe vera* extract, which reduced and stabilized AuNPs, and studied their physicochemical properties under different physiological conditions.²⁶ They

Received: October 8, 2022

Accepted: January 5, 2023

Published: February 8, 2023



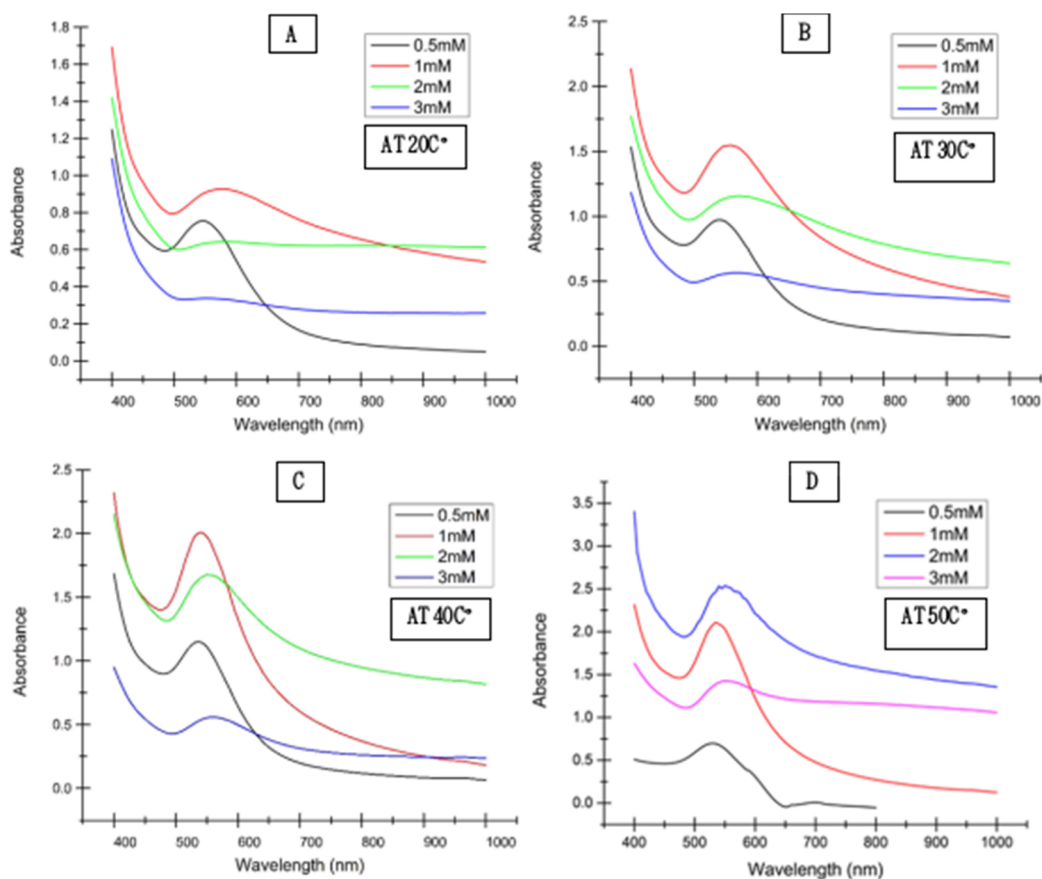


Figure 1. (A–D) UV/vis spectrum of AuNPs prepared from *Aloe vera* gel extract against different salt concentrations and temperatures.

have reported stable complexes at neutral or slightly acidic pH ranges. Philip used honey for the green production of AuNPs for the first time.²⁷ The author found that the reduction was probably due to fructose followed by protein stabilization of the NPs. Nakkala et al. produced silver and gold NPs using *Gymnema sylvestre* extract.²⁸ They found that the synthesized NPs exhibited substantial antioxidant activity and toxicity against the Hep2 cell line. A detailed review of other studies on plant-based reduction of silver and gold NPs can be found elsewhere.²⁹ Despite its significance, very few reports have been presented on the green synthesis of AuNPs using plant extracts. Furthermore, no comparative study exists on the chosen sources as done in this study. Excessive data are available regarding the synthesis of AuNPs from organic sources, which proves the essentialities associated with organic methods of synthesis. However, we found a gap in the literature pertaining to the most appropriate physicochemical parameters that are useful for the synthesis protocols of selected organic sources. To overcome the gap, this study focused on the effect of different parameters such as precursor concentration and temperature to get optimized conditions for the preparation of AuNPs with controlled size and morphology.

In this study, AuNPs were synthesized using raw honey, leaf extracts of *Gymnema sylvestre*, and *Aloe vera* gel at varying temperatures, and gold salt concentrations. Green synthesis of AuNPs from these sources was chosen to overcome the limitations such as cytotoxicity, high cost, and environmental pollution. These parameters strongly influence the distribution of the size and shape and hence their physicochemical properties of NPs.^{30,31} AuNPs were further characterized via ultraviolet–

visible (UV–vis) spectroscopy, X-ray diffraction (XRD), Fourier transform infrared (FTIR) spectroscopy, and scanning electron microscopy–energy-dispersive X-ray spectroscopy (SEM–EDX) and checked for their antioxidant properties. Finally, these nanoparticles were coated with polyethylene glycol (PEG) followed by conjugation with three FDA-approved anti-cancerous drugs 4-hydroxy Tamoxifen, HIF1- α inhibitor, and ODQ, and their anti-cancerous effects were assessed on MCF-7 and MDA-MB-231 cell lines. The results have been analyzed to help future research on anti-cancerous drug delivery vehicles and to modify the targeted drug delivery protocols.

2. RESULTS AND DISCUSSION

2.1. Effect of the Gold Salt Concentration and Temperature on AuNP Synthesis. The size distribution and physicochemical properties of NPs depend on parameters such as metal salt concentrations, varying temperatures, pH, reaction time, and concentration of reducing agents. In a traditional approach, one factor is varied at a time while keeping all other factors constant. Four different concentrations of gold salt were incubated with the extract of each biological source. These reaction mixtures were incubated at different temperatures to optimize the conditions for the formation of AuNPs by these sources. The initial transparent to pale-yellow color of the reaction mixture was noted at time $t = 0$. The reduction of gold ions was monitored through the color change of the reaction mixtures after 24 h. This color change from pale yellow to brown and dark purple demonstrated the formation of AuNPs^{32,33} from *Aloe vera*, honey, and *Gymnema sylvestre* leaf extract (GYLE) (Figure S1A–C). In contrast, control samples with pure extract

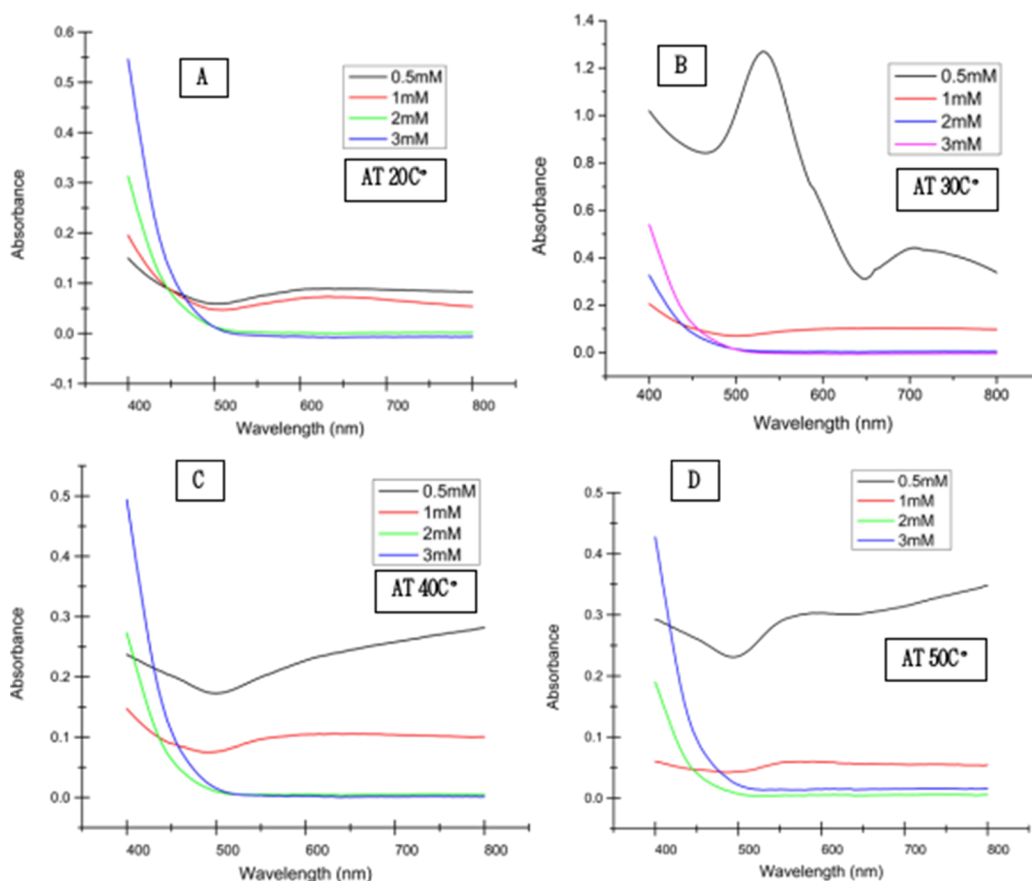


Figure 2. (A–D): UV/vis spectrum of AuNPs prepared from *Honey* against different salt concentrations and temperatures.

of the sources or HAuCl_4 showed no change in color when incubated under similar conditions. The sample of *Aloe vera* gel extract incubated with 1 and 2 mM gold salt solution at 40 and 50 °C showed a grayish-purple color (Figure S2A and Table S1). Contrarily, honey extract incubated with 0.5 mM gold salt solution at 30 °C demonstrated a color change from pale yellow to reddish-purple, (Figure S2B). GYLE showed a desired color change to wine and brownish red when incubated with 1 and 2 mM gold salt solution at 30 and 40 °C (Figure S2C) respectively. The GYLE and honey extracts reduced the gold ions, Au^{3+} , to Au^0 due to the presence of one or more oxidizable molecule(s) in the reaction mixtures under the desired physiological conditions.³⁴

2.2. Characterization of AuNPs. **2.2.1. UV–Vis Spectral Analysis.** The controls consisting of *Aloe vera* gel extract, honey, and GYLE, and the reaction mixtures incubated for 24 h with different concentrations of salt solutions and varying temperatures were subjected to UV–vis spectroscopy with wavelengths ranging from 200 to 800 nm. The controls showed no peak around 500 nm, which is a region of interest for AuNPs, as shown in Figure S2. The absorbance peak observed in the wavelength region of 500–570 nm for the synthesized AuNPs from three different sources is due to the collective oscillation of electrons on their surface caused by the surface plasmon resonance (SPR) phenomenon.³⁵ Furthermore, a single peak indicates spherical-shaped NPs while the occurrence of two or more plasmon bands represents the anisotropic shape of the AuNPs.³⁶

2.2.2. Optimization of Physio-Chemical Parameters for AuNP Biosynthesis. High temperatures increase the reaction

rate for the uniform synthesis of AuNPs.³⁷ Moreover, the geometry and dimension of the NPs are defined by each physical and biological parameter. Cell-free extracts are sources of reducing and stabilizing agents, which can affect the growth and nucleation of NPs. A higher concentration of reducing agents can be attributed to the high concentration of proteins coming from the extract.³⁸ In contrast, an increased concentration of gold ions in the reaction mixture produces nanoparticles which are thermodynamically unstable.³⁹ In the case of *Aloe vera* gel extract, the temperature played a critical role in determining the best condition for the synthesis of AuNPs, analyzed by UV/Vis spectroscopy (Figure 1A–D). It can be observed that as the temperature of the reaction mixture increases, the absorbance also increases, indicating a high yield of AuNPs. The increase in absorbance with increasing temperature was similar for AuNPs synthesized from 1, 2, and 3 mM salt solution concentrations except for 0.5 mM concentration where its absorbance decreased at 50 °C (Figure 1D). Overall, the best reaction temperatures were 40 and 50 °C (Table S1), and the optimum gold salt solution concentrations were 1 and 2 mM.

Similar reaction patterns were observed for AuNPs prepared from the honey extract and the results of UV–vis in this case are shown in Figure 2A–D. The details of the reaction mixture responding to varying temperatures and molarity of gold salt solution can be observed in Table S1 (Supplementary Material). In the case of honey, only 0.5 mM gold salt concentration at 30 °C temperature gave the best peak (Figure 2B). Therefore, both these conditions were selected for further synthesis of AuNPs from the honey extract. Honey is a complex material containing 400 different compounds including alcohols, ketones, aldehydes,

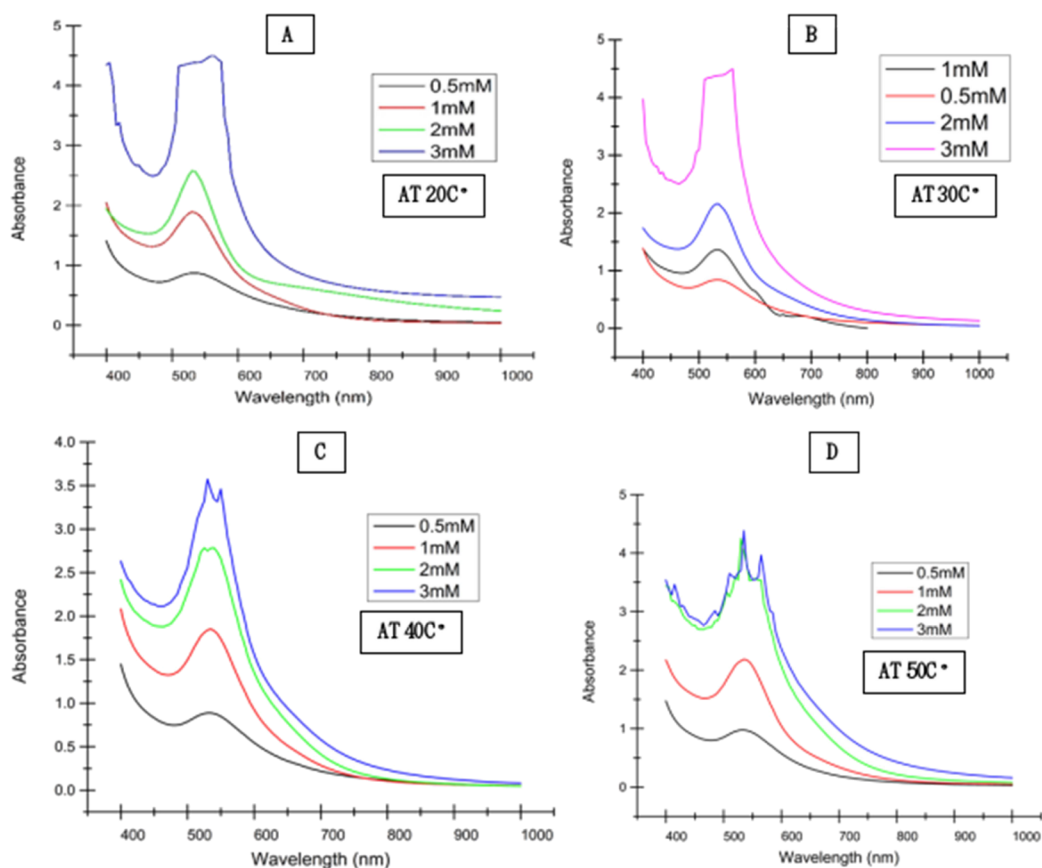


Figure 3. (A–D): UV/Vis spectrum of AuNPs prepared from GYLE against different salt concentrations and temperature.

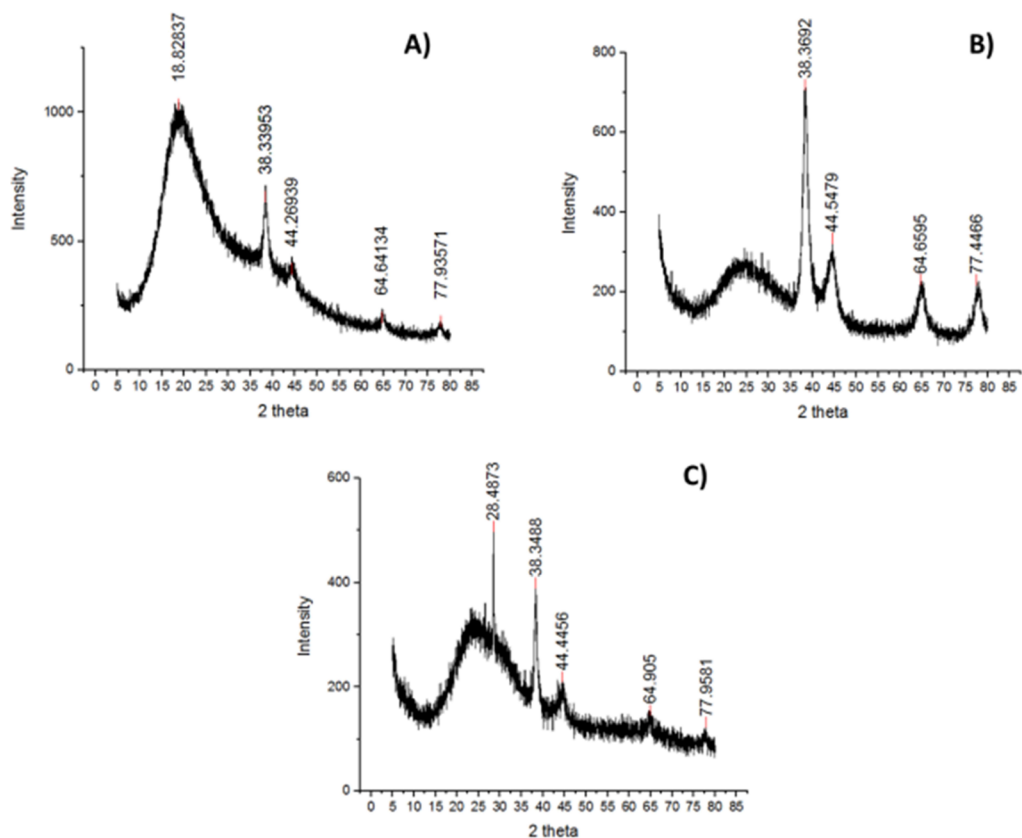


Figure 4. Comparison of XRD spectra of AuNPs synthesized from different sources. *Aloe vera* (A), honey (B), and GYLE (C).

Table 1. Miller Indices, Crystallite Size, Lattice Parameter, and Lattice Strain for All the Samples Calculated from the XRD Data

sample	angles corresponding to the (<i>hkl</i>) indices				crystallite size (Å)	$d_{hkl} = \lambda/2\sin\theta$ (Å)	lattice parameter, $a = d_{hkl} * \sqrt{(h^2 + k^2 + l^2)}$ (Å)
	(111)	(200)	(220)	(311)			
<i>Aloe vera</i>	38.34	44.27	64.64	77.94	78.524	2.346	4.063
honey	38.37	44.55	64.66	77.45	78.527	2.345	4.062
<i>G. Sylvester</i>	38.35	44.45	64.91	77.96	188.136	2.346	4.063

acids, terpenes, hydrocarbons, benzene, and furan derivatives. However, the two main monosaccharides, fructose and glucose, in honey act as reducing agents. Therefore, honey-reduced nanoparticles existed in various shapes and sizes.⁴⁰

UV/vis spectroscopic analysis of AuNPs synthesized from GYLE (Figure 3A–D) showed that the effect of varying molarities of the gold salt solution is more prominent at different temperatures of the reaction mixture. At all four temperatures, the absorbance of the AuNPs increased with increasing gold salt concentration up to 2 mM. Overall, the results showed that the optimum salt concentration for the high yield synthesis of AuNPs from GYLE was 1 and 2 mM at 30 and 40 °C, respectively. Details of various reaction mixtures have been elaborated in Table S1 (Supplementary material). Interestingly, GYLE-reduced AuNPs showed a weak shoulder around 650–700 nm, which is an indication of anisotropic particles.

2.2.3. XRD Analysis. Figure 4 shows the XRD spectrum graph of the three best samples chosen after the optimization of physicochemical experiments. The graph represents 2θ values of 38.34, 44.27, 64.64, and 77.94° corresponding to crystalline planes (111), (200), (220), and (311) facets, respectively. The peaks are slightly shifted toward larger 2θ values in the case of nanoparticles synthesized from honey, which indicates a decrease in the lattice constant.

The lattice constants for the three samples have been calculated and are presented in Table 1. The calculated lattice constants are close to the value reported previously.²⁸ The broad amorphous peaks below 20° correspond to the (100) facet of SiO₂ due to the inhomogeneous coverage of the glass substrate.

2.2.4. SEM Analysis. SEM analysis confirmed the size and shape of the NPs synthesized by three sources. The AuNPs synthesized from *Aloe vera* gel extract were observed to be uniformly dispersed and spherical with the diameter ranging from 30 to 45 nm (Figure 5A–C). AuNPs synthesized from honey were of varying sizes and shapes; large-sized gold nanocubes and small-sized gold nanospheres are shown in Figure 5B. This can be attributed to the simultaneous reduction of AuNPs by fructose and glucose in honey. For instance, the growth of more intricate nanostructures such as nanotriangles and nanoprisms has been reported using honey.⁴⁰ The reaction kinetics of such systems can be described by the stretched exponential function. Furthermore, a few nanocube dimers (indicated by yellow circles) were also observed in the sample. AuNPs synthesized from GYLE were spherical with an average particle size of 30–40 nm (Figure 5A–C). GYLE is known for its free radical scavenging ability. The antioxidant activity of GYLE-reduced AuNPs has been already reported previously.⁴¹ These NPs have shown remarkable cytotoxicity against Hep2 cells. Optimized reaction conditions may lead to the controlled agglomeration of NPs which may prove to be beneficial for long-term storage and sensing applications.⁴² GYLE-reduced AuNPs also exhibited dimer formation, as indicated by yellow circles in Figure 5C.

2.2.5. EDX Analysis. EDX spectroscopy of AuNPs was performed for all the samples shown in Figure 6A–F. The

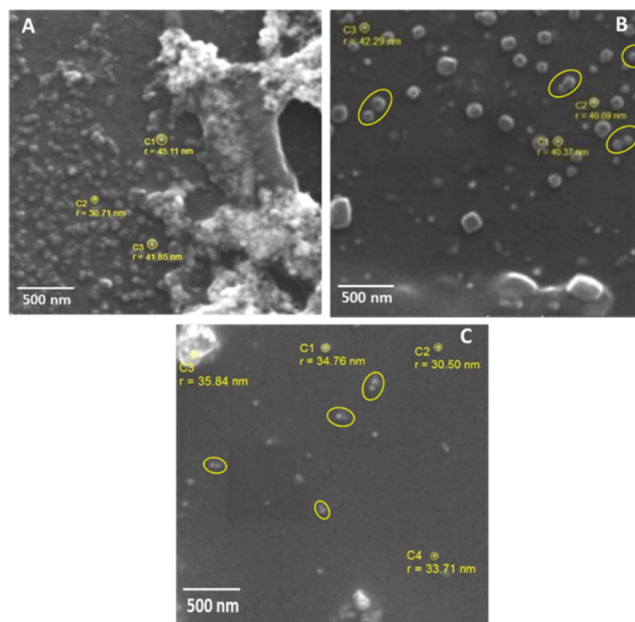


Figure 5. SEM images of AuNPs derived from *Aloe vera* extract (A), honey (B), and GYLE (C).

corresponding percentage weight for Au in *Aloe vera*, honey, and GYLE-derived AuNPs was found to be 21, 25.8, and 34.68%, respectively.

2.2.6. FTIR Analysis. FTIR analysis was conducted to evaluate different functional groups in the samples. These functional groups, present in chemicals and enzymes, are required for the biosynthesis of NPs because they act as stabilizing and capping agents for them. The functional groups encompassing AuNPs derived from the *Aloe vera* gel extract showed sharp bands at 1627, 3423, and 3562 cm⁻¹ representing the stretching vibrations of the amine group (N–H) and alcohol group (O–H); while medium broad and weak bands at 1101 and 2906 cm⁻¹ depict aliphatic ether (C–O) stretching and alkane (C–H) stretching vibration, respectively (Figure 7).

In the case of AuNPs synthesized from honey, bands shown at 3440.8 cm⁻¹ are due to the stretching vibration of the aliphatic primary amine group (N–H). The band at 2347 cm⁻¹ represents (C=O=C) stretching. Bands for primary alcohol (C–H) appear at 2395 cm⁻¹. C=O represents the carbonyl group in the amide linkage in proteins. A sulfate linkage is present due to sulfur-containing amino acid residues at 1057 cm⁻¹. Microbial-mediated AuNPs possess a binding affinity to amides and thiols, present in proteins. The presence of these functional groups confirms that free amino groups can form a capping layer on AuNPs, thus preventing them from agglomeration (Figure 7).

For AuNPs derived from GYLE, the band shown at 3445 cm⁻¹ is due to the stretching vibration of alcohols (O–H) that shows strong bonding and the band appeared is broad. Bands for primary alcohol (C–H) appear at 2892 cm⁻¹. The band at 2078

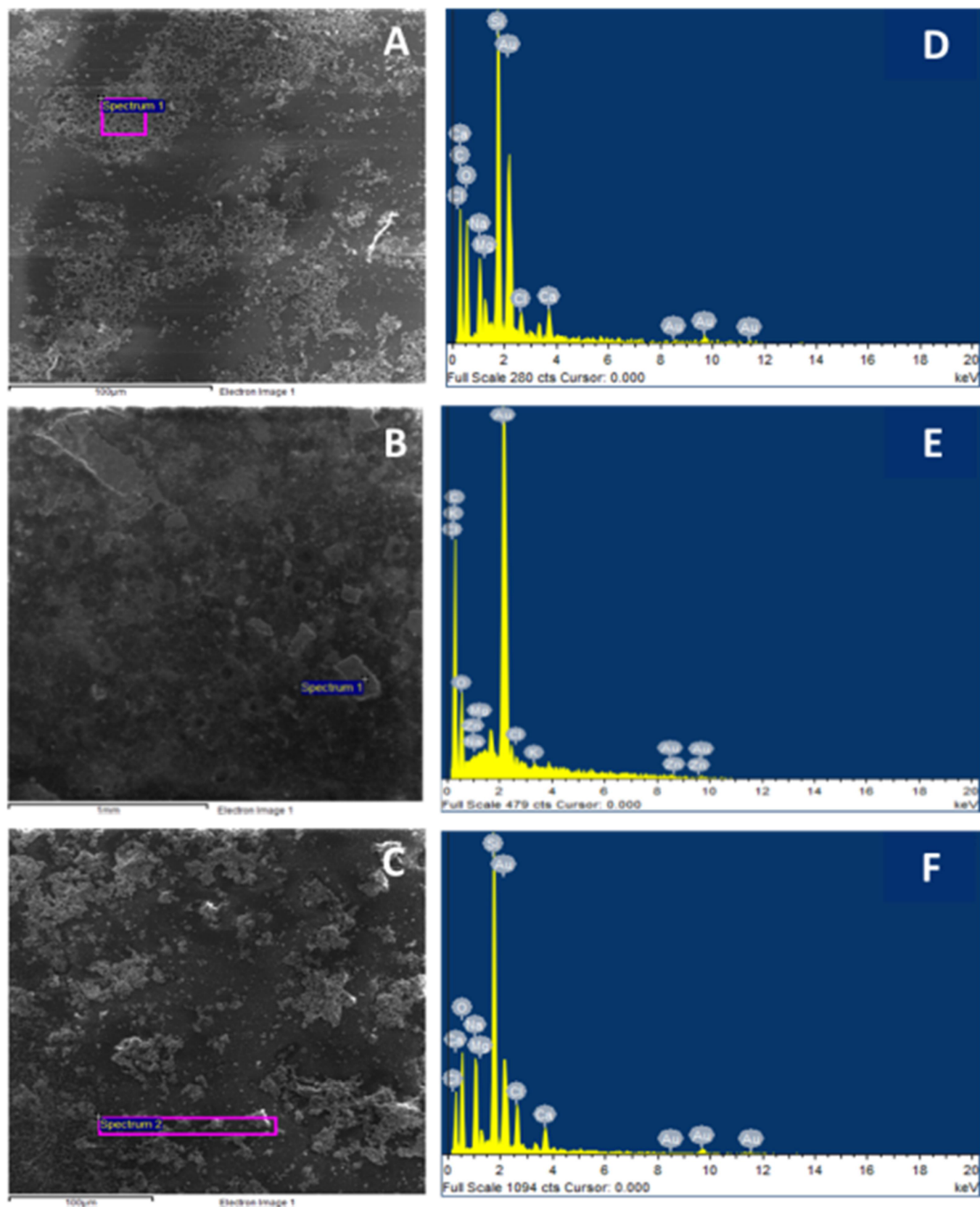


Figure 6. (A–F) EDX analysis of all the samples. (A–C) SEM images of AuNPs synthesized from *Aloe vera*, honey, and GYLE, respectively. D–F represent the corresponding EDX micrographs for the three samples.

cm^{-1} represents (N=C=S) stretching, which indicates an isothiocyanate group with strong bonding. C=C represents the conjugated alkene group in amides linkage in proteins. Halo

compound (C–Br) stretching is seen at 649 cm^{-1} due to the initial mixing of the sample with KBr.

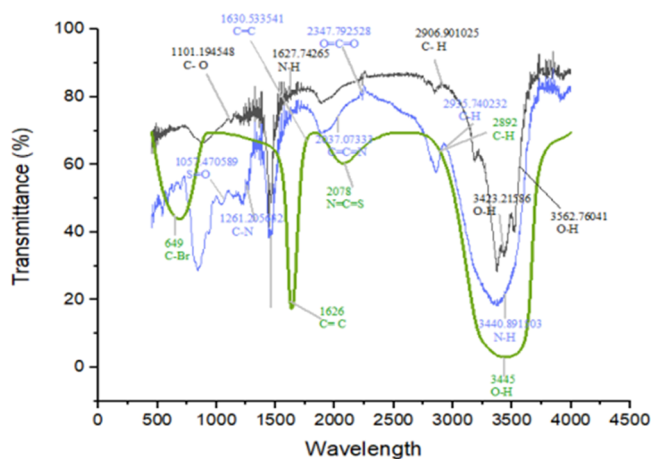


Figure 7. Infrared spectra of AuNPs synthesized from *Aloe vera*, honey, and GYLE. *Aloe vera* (black line), honey (blue), and GYLE (green).

The alcohol functional group is present in all the samples. Amine appeared as a functional group in honey and *Aloe vera*-derived AuNPs. Alkane and aliphatic ether functional groups were unique to the *Aloe vera*-derived AuNPs while carbonyl and sulfate groups were features of AuNPs synthesized using honey. As for GYLE-synthesized AuNPs, isothiocyanate and alkene groups had distinct characteristics, while Halo compound (C–Br) stretching was seen at 649 cm^{-1} which was due to the initial mixing of the sample with KBr for processing. These groups prevent AuNPs from agglomeration due to the capping of free amino groups on AuNPs and provide stability to the biosynthesized gold nanoparticles (Figure 7).

2.3. Antioxidant Activity. **2.3.1. DPPH Assay.** Results of the DPPH assay revealed that the scavenging ability of AuNPs and ascorbic acid increases with the increased concentration of AuNPs and ascorbic acid. AuNPs prepared from *Gymnema*, honey, and *Aloe vera* showed a maximum of ~ 83.29 , 90.4 , 9 , and 93% scavenging ability at $2000\text{ }\mu\text{g/mL}$, respectively, as compared to 94.4% of the maximum scavenging ability shown by ascorbic acid (positive control). These results showed that AuNPs possess significant antioxidant ability compared with the natural antioxidants, but there exists a significant difference in their percentage scavenging activities. Figure 8 shows the scavenging ability of *Aloe vera*, honey, and *Gymnema sylvestre* AuNPs against ascorbic acid at the 517 nm range (Figure 8).

2.4. Drug Conjugation: Confirmation of PEGylation and Drug Conjugation. (Z)-4-Hydroxytamoxifen, Hypoxia Inducible Factor-1 alpha (HIF-1-alpha) Inhibitor, and H-[1, 2, and 4] oxadiazole [4, 3, -a] quinoxaline-1 (ODQ) were used to

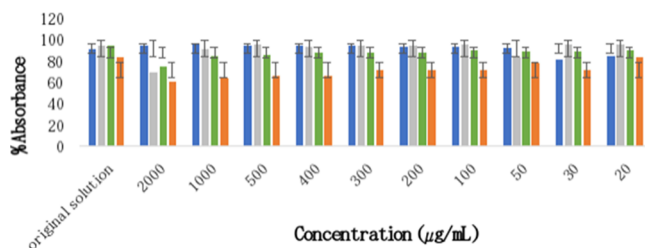


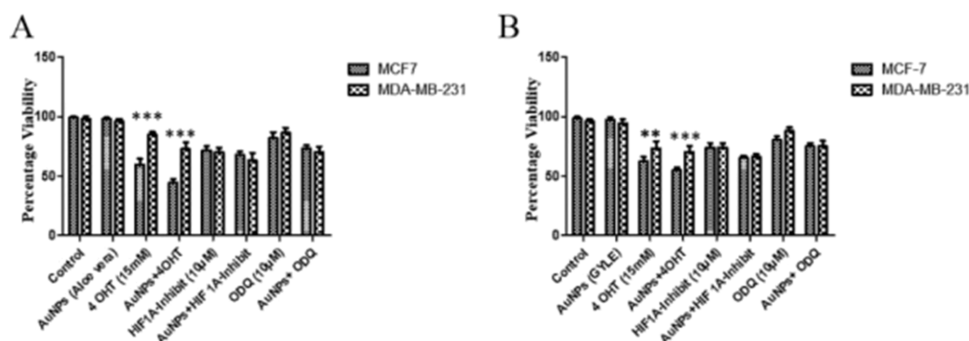
Figure 8. DPPH assay showing percentage radical scavenging activity of different conc. of ascorbic acid vs AuNPs prepared from all three biological sources. Blue line for (ascorbic acid), gray (*Aloe vera*), green (honey), and orange (*Gymnema sylvestre*).

treat breast cancer. One milliliter of (10% PEG) was added to 9 falcon tubes containing 5 mL of NP pellet suspension mixed well through vortex mixing at a high speed. The PEGylation of the prepared NPs was confirmed through a peak shift of the plasmonic peak at $540\text{--}560\text{ nm}$. However, PEGylation was unsuccessful in all 9 reaction tubes since no specific increase in the absorbance value was observed in any reaction tubes. After thorough vortex mixing of pellets and probe sonication, the pellets containing PEG and bound drugs were suspended in deionized water. Both pellet solutions along with the separated supernatant solution were checked under UV–vis. An increase in the size of AuNPs from 540 to $550\text{--}560\text{ nm}$ (PEGylated NPs) and finally to $570\text{--}580\text{ nm}$ (drug-conjugated NPs) confirmed the conjugation of drugs.

2.5. Cytotoxicity Assay. MCF7 (ATCC-HBT-22) and MDA-MB-231 (ATCC-HTB-26) cell lines are both invasive ductal carcinoma breast cells. MCF7 cells are estrogen and progesterone receptor positive and respond to the selective estrogen receptor modulator tamoxifen while the MDA-MB-231 cell line is of triple-negative breast cancer. The lack of estrogen receptor has rendered MDA-MB-231 insensitive to antiestrogen treatments widely used in breast cancer endocrine therapies.^{43–45} MCF7 cells rely on ATP production from oxidative phosphorylation under normoxic conditions but increase their glycolytic activity under hypoxia, whereas MDA-MB-231 cells rely on glycolysis for ATP production under both normoxic and hypoxic circumstances.⁴⁶ The AuNPs generated from *Aloe vera* and GYLE were conjugated with (Z)-4-Hydroxytamoxifen, Hypoxia Inducible Factor-1 (Alpha) (HIF-1-alpha) inhibitor, and H-[1, 2, and 4] oxadiazole [4, 3, -a] quinoxaline-1 (ODQ) for targeted delivery of drugs to breast cancer cells by reducing cytotoxicity against normal cells. For control, saline in the media, unbound drugs, and AuNPs alone, while for treatment, AuNPs conjugated with these drugs individually were used. AuNPs derived from both *Aloe vera* and GYLE did not show any cytotoxic effects and hence proved to be biologically safe. In the case of AuNPs derived from *Aloe vera*, a significant difference was observed in the case of (Z)-4-Hydroxytamoxifen-treated cell lines ($P < 0.001$ ***) and (Z)-4-Hydroxytamoxifen conjugated with GYLE AuNP-treated cell lines ($P < 0.001$ ***), and other free or conjugated drugs comparatively induced no significant difference in both cell lines (Figure 9). In the case of AuNPs derived from GYLE, a significant difference was observed in (Z)-4-Hydroxytamoxifen-treated cell lines ($P < 0.01$ **) and (Z)-4-Hydroxytamoxifen conjugated GYLE AuNP-treated cell lines ($P < 0.001$ ***) compared with GYLE AuNPs free and conjugated with other drugs.

3. DISCUSSION

This research was a part of a comprehensive study and its aim was to compare different methods for the formation of AuNPs to establish the best method. Evidently, three sources were used to synthesize AuNPs from a biological source, i.e., *Gymnema sylvestre* extract, *Aloe vera* gel extract, and raw honey. All these sources showed very similar results, i.e., a good yield of mono-dispersed AuNPs with ease of synthesis and without the addition of harmful chemicals for reduction, capping, or functionalization of AuNPs. These NPs were highly stable at elevated temperatures for a long time. This was established by autoclaving the reaction solutions before characterization and biological activity analysis and the results are still outstanding. While conducting the analysis of physicochemical parameters for the formation of AuNPs from different concentrations of chloroauric acid



forth a doorway for cancer biologists to further work on conjugation protocols of anti-cancerous drugs with AuNPs to carry further experiments for targeted drug therapeutics designs. Studies should continue on the highlighted domain of science, so that in future, better therapeutic options are availed for the reduction of cancer-associated healthcare burden.

Furthermore, AuNPs were also conjugated with three anticancer drugs, namely, ((Z)-4-Hydroxytamoxifen, Hypoxia Inducible Factor-1 (Alpha) (HIF-1-alpha) Inhibitor, and H-[1, 2, and 4] oxadiazole [4, 3, -a] quinoxalin-1 (ODQ)). UV-vis spectral analysis revealed that these AuNPs can carry anticancer drugs and therefore can act as anticancer drug carriers for targeted treatment of breast cancer. For future studies, it is highly crucial to develop uniformly sized and shaped AuNPs, with enhanced and long-term stability along with biological safety, and adjustable features to ensure the synthesis of best candidates for the nanotechnology-based development of healthcare practices and more effective and personalized nanomedicine in future.

5. EXPERIMENTAL SECTION

5.1. Materials. Chloroauric acid ($\text{HAuCl}_4 \cdot 3\text{H}_2\text{O}$, 99.99%), potassium bromide (KBr, 99%), polyethylene glycol 6000 (PEG), 2,2-diphenyl-1-picrylhydrazyl (DPPH) (99%), 3-(4,5-dimethyl-2-thiazolyl)-2,5-diphenyl-2H-tetrazolium bromide (MTT), 4-(1-[4-(dimethyl aminoethoxy) phenyl]-2-phenyl-1-butenyl) phenol (4 Hydroxy Tamoxifen) were purchased from Sigma-Aldrich, USA. Solvents such as methanol (99%), ethanol (99%), phosphate buffer, RPMI 1640 media, penicillin-streptomycin (10,000 U/mL), and fetal bovine serum (FBS) were purchased from Fisher Scientific, UK. HIF-1-alpha inhibitor and ODQ (1H-[1,2,4]oxadiazolo [4,3, -a] quinoxaline-1) were purchased from Chem Cruz, USA.

5.2. Synthesis of AuNPs from the Aloe vera Gel Extract. The *Aloe vera* leaves were peeled to collect the viscous gel. This gel was blended to get a uniform texture. A 30% dilution of the gel was prepared by adding 30 mL of the gel in 70 mL of distilled water which was boiled at 100 °C for 5–10 min and filtered via Whatman filter paper to get the *Aloe vera* gel extract. In a conical flask, 10 mL of the gel extract was reacted with 10 mL of four different concentrations (0.5–3 mM) of $\text{HAuCl}_4 \cdot 3\text{H}_2\text{O}$. The reaction mixtures were incubated at different incubation temperatures (20–50 °C) to optimize conditions for the formation of AuNPs. Thereafter, the flasks were shaken at a rotation rate of 150 rpm in the dark. The color change of the reaction mixture from pale brownish to purple color was observed.

5.3. AuNP Synthesis from Honey. Organic honey with no added preservatives was obtained from a local market in Islamabad, Pakistan. The extract was prepared by dissolving 1 mL of honey with 50 mL of distilled water in an Erlenmeyer flask followed by heating on a hot plate with a magnetic stirrer at 60 °C. A total of 16 reaction tubes containing 10 mL of honey extract were incubated at 20–50 °C with four different concentrations (0.5–3 mM) of $\text{HAuCl}_4 \cdot 3\text{H}_2\text{O}$ and shaken at a rotation rate of 150 rpm in the dark.

5.4. Synthesis of AuNPs from *Gymnema sylvestre* Leaf Extract. The leaves were washed with distilled water followed by oven-drying at 40 °C (ULE-500, Memmert, Germany). Subsequently, the leaves were ground into a fine powder using an electric blender (SM-2460, Sanyo, Japan). To prepare the aqueous GYLE, one gram of its fine powder was mixed with 100 mL of double-distilled water in a 250 mL Erlenmeyer flask and

boiled at 60 °C for 30 min on a hot plate with a magnetic stirrer (US152, Buch Holm, USA). The crude aqueous extract was filtered using Whatman filter paper No. 1 and stored at 4 °C for further experimentation.¹⁹ For biological synthesis of AuNPs, 6 mL of GYLE was mixed with four different concentrations of gold salt solution at four different temperatures, as mentioned in Sections 5.3 and 5.4.

5.5. Characterization of AuNPs. **5.5.1. UV-Vis Spectroscopy.** The reduction of the Au^{3+} ions was monitored by measuring the UV-vis spectra of the aliquots of reaction mixtures in a quartz cuvette at regular intervals on a UV-1650CP Shimadzu spectrophotometer at a wavelength ranging from 300 to 800 nm. For baseline correction, deionized water was used as blank.

5.5.2. X-ray Diffraction. XRD characterization was conducted to determine the crystal structure of AuNPs using D8 Advance, BRUKER, Diffractometer, Germany. When an incident X-ray beam is directed at the sample at a different range of angles, it is diffracted in different directions due to the crystalline structure of the material under investigation. The sample on a glass slide was scanned at a 2θ range of 20–80° with time and an increment of 0.02°/0.1 s interval. A voltage of 40 kV and 40 mA current were applied with Cu-K α radiation ($\lambda = 1.54 \text{ \AA}$) in the instrument. An average crystallite diameter was measured from scanned samples using the Debye-Scherrer equation:

$$D = 0.9\lambda/\beta\cos\theta \quad (1)$$

D (nm) is the size, λ (nm) is the wavelength of Cu-K α radiation, β (radians) is the full width at half maximum (FWHM), and θ (radians) is the half of the Bragg angle.

5.5.3. Scanning Electron Microscopy. The morphology of the bioreduced AuNPs and their size were studied by SEM (VEGA3, TESCAN, Czech Republic) using a beam of electrons focused on the samples. The samples were sonicated (EW-04711-35 Ultrasonicator, Cole Parmer, USA) for 1 h at 37 °C to avoid the aggregation of AuNPs. The accelerating voltage of the microscope was set at 20 kV and a working distance of 15 mm for the sample was chosen.

5.5.4. Energy Dispersive Spectroscopy. The elemental composition of biologically synthesized AuNPs was determined by EDX equipped in SEM between the energy range of 0–20 keV.

5.5.5. Fourier Transform Infrared Spectroscopy. FTIR spectra show a wavenumber shift of the functional groups of extracts before and after the formation of AuNPs in the mixture. A Perkin-Elmer Spectrum-100 spectrometer, USA, was used to detect the presence of different types of functional groups on the surface of Au-NPs present in the reaction mixture. Liquid sample aliquots were mixed with KBr, a hygroscopic chemical, to remove moisture from samples and were oven-dried at 200 °C for 30 min. Fine powder of KBr mixed samples was obtained by grinding manually in a pestle and mortar. A range of 4000–350 cm^{-1} infrared wavelength and 4 cm^{-1} resolution was applied to the powder fixed in the pellet holder.

5.6. Determination of Antioxidant Activity. **5.6.1. DPPH Free Radical Scavenging Assay.** Antioxidant activity of selected AuNPs from different sources, each having different concentrations and incubation temperatures was determined by DPPH (2, 2-diphenyl-1-picrylhydrazyl) assay according to a standard procedure.⁴⁷ The principle of this colorimetric method is a color change observed via UV-vis spectrophotometry at 517 nm as a result of the reduction of hydrogen donors or antioxidants

present in a sample. Briefly, 1 mM DPPH was prepared in methanol. Aliquots of 1.6 mL having varying concentrations of AuNPs (20–2000 $\mu\text{g}/\text{mL}$) in distilled water were added to 0.4 mL of 0.1 mM DPPH. The reaction mixture was vortexed properly and incubated at 37 °C in dark for a maximum of 30 min while shaking at 100 rpm. The following formula (eq 2) was used to determine the percentage scavenging radical potential of AuNPs from different sources.

$$\% \text{Inhibition} = [(A_{\text{control}} - A_{\text{sample}}) / A_{\text{control}}] \times 100 \quad (2)$$

where A_{control} is the absorbance value of the control and A_{sample} is the absorbance value of the test sample. Ascorbic acid was used as a reference and tests were conducted in triplicate.

5.7. Conjugation of Drugs with AuNPs. *5.7.1. Selection of Similar-Sized Nanoparticles via Differential Centrifugation.* Synthesized AuNPs were further used for the conjugation of (Z)-4-hydroxytamoxifen, Hypoxia Inducible Factor-1 (Alpha) (HIF-1-alpha) Inhibitor, and H-[1, 2, and 4] oxadiazole [4, 3, -a] quinoxaline-1 (ODQ). For the separation of uniform size AuNPs, differential centrifugation was carried out at 500, 1000, and 2000 r.c.f which gave different pellets. These pellets were resuspended in 5 mL of deionized water after removing the supernatant with each progressive step. After completing the centrifugation at 3 different speeds, we concluded that the second round of centrifugation at 1000 r.c.f gave the best results in the form of thick visible and measurable pellets and light color of the supernatant as an indication that most of the identical-sized NPs have been settled down. Thus, these pellets at 1000 r.c.f were chosen for further experimentations of drug conjugation.

Stock solutions of 50 $\mu\text{g}/\text{mL}$ of all drugs, HIF-1-alpha Inhibitor, ODQ, and 4-hydroxy Tamoxifen were prepared. AuNP emulsions prepared from three different biological sources were centrifuged at 500 rpm for 30 min at 4 °C. The supernatant was shifted to another falcon tube and again centrifuged at 1000 rpm at 4 °C for 30 min. Centrifugation results in the separation of particles of uniform size from the heterogeneous emulsion. The pellet of AuNPs obtained after the second centrifugation was resuspended in 20 mL of deionized water. Subsequently, 5 mL of AuNPs solution was shifted to six falcon tubes labeled with anticancer drugs. PEG 60 μL was added to each AuNPs tube, thoroughly mixed for 5 min on a vortex at 250 rpm, and added to a cuvette to determine the absorbance of Au-NP-PEG solution via a UV-vis spectrophotometer. Thereafter, 5 mL of 50 $\mu\text{g}/\text{mL}$ of each drug was added to the six falcon tubes bearing AuNP-PEG solution tubes were vortexed for 5 min and then sonicated for 2 min. These AuNP-PEG-drug solutions were transferred to a cuvette to determine the absorbance. The sample tubes were centrifuged at 6300 rpm for 30 min at 4 °C and the supernatant was shifted to a cuvette to determine the absorbance of the unbound drug remaining in the supernatant via the UV-vis spectrophotometer while the bound drug remained in the pellet. The pellet was resuspended in 5 mL of deionized water and stored in dark conditions at 4 °C.

5.8. Cytotoxicity Assay. MCF7 (ATCC HTB-22) and MDA-MB-231 (ATCC HTB-26) cells were cultivated in RPMI 1640 supplemented with 10% fetal bovine serum and 1% of penicillin-streptomycin. Cells were incubated at 37 °C under 95% moisturized air with 5% CO_2 . Before the experiment, cells were trypsinized (0.25% Trypsin and EDTA) and seeded (1×10^4 cells/well) on 96-well plates. The AuNPs, free and conjugated drugs were measured using 5 mg/mL 3-(4,5-dimethyl-2-thiazolyl)-2,5-diphenyl-2H tetrazolium bromide

(MTT) assay. The cells were treated with AuNPs, drug-loaded AuNPs, and drugs only for 24 h. Cells were once again incubated for 48–72 h followed by the addition of 10 μL of the prepared MTT solution in each well. The plate was then incubated for three more hours before 100 μL of DMSO was added. Absorbance was subsequently recorded in a microplate reader at 570 nm. MTT assay results were evaluated using the following formula (eq 3):

$$\begin{aligned} \% \text{cell survival} &= \frac{[\text{absorbance of sample} - \text{absorbance of blank}]}{[\text{absorbance of control} - \text{absorbance of blank}]} \\ &\times 100 \end{aligned} \quad (3)$$

$$\% \text{cell inhibition} = 100 - \% \text{cell survival}$$

5.9. Statistical Analysis. The results of experiments performed in triplicate were expressed as mean \pm standard deviation and a two-way analysis of variance (ANOVA) was used to determine the statistical significance of differences with the help of the SPSS 17.0 statistical software and GraphPad Prism 7.0.

■ ASSOCIATED CONTENT

SI Supporting Information

The Supporting Information is available free of charge at <https://pubs.acs.org/doi/10.1021/acsomega.2c06491>.

Additional figures as mentioned in the text (PDF)

■ AUTHOR INFORMATION

Corresponding Authors

Faheem Amin – Department of Physics, School of Natural Sciences (SNS), National University of Sciences and Technology (NUST), Islamabad 46000, Pakistan; orcid.org/0000-0003-3961-837X; Email: faheemamin@sns.nust.edu.pk

Rumeza Hanif – Atta-ur-Rahman School of Applied Biosciences (ASAB), National University of Sciences and Technology (NUST), Islamabad 44000, Pakistan; Email: rumeza.hanif@asab.nust.edu.pk

Authors

Shiza Malik – Atta-ur-Rahman School of Applied Biosciences (ASAB), National University of Sciences and Technology (NUST), Islamabad 44000, Pakistan

Maha Niazi – Atta-ur-Rahman School of Applied Biosciences (ASAB), National University of Sciences and Technology (NUST), Islamabad 44000, Pakistan

Maham Khan – Atta-ur-Rahman School of Applied Biosciences (ASAB), National University of Sciences and Technology (NUST), Islamabad 44000, Pakistan

Bisma Rauff – Department of Biomedical Engineering, University of Engineering and Technology (UET), Lahore 53400, Pakistan; Present Address: Westmead Institute for Medical Research, University of Sydney NSW, Sydney 2006, New South Wales, Australia

Sidra Anwar – Atta-ur-Rahman School of Applied Biosciences (ASAB), National University of Sciences and Technology (NUST), Islamabad 44000, Pakistan

Complete contact information is available at:

<https://pubs.acs.org/10.1021/acsomega.2c06491>

Notes

The authors declare no competing financial interest.

ACKNOWLEDGMENTS

We are thankful to the Higher Education Commission (HEC), Pakistan, for funding the research project 9874, "Gold nanoparticles as a targeted drug delivery vehicle in breast cancer therapy."

REFERENCES

- (1) Li, X.; Cao, Z.; Liu, R.; Liu, L.; Li, H.; Li, X.; Chen, Y.; Lu, C.; Liu, Y. AuNPs are important inorganic nanoparticles applied in drug carrier systems. *Artif. Cells Nanomed. Biotechnol.* **2019**, *47*, 4222–4233.
- (2) Cui, H. D.; Hu, D. H.; Zhang, J. N.; Gao, G. H.; Zheng, C. F.; Gong, P.; Xi, X. H.; Sheng, Z. H.; Cai, L. T. Theranostic gold cluster nanoassembly for simultaneous enhanced cancer imaging and photodynamic therapy. *Chin. Chem. Lett.* **2017**, *28*, 1391–1398.
- (3) Yang, J.; Nian, F.; Guo, Z.; Bai, T.; Peng, G. The effect of gold nanoparticles with different diameters on rat neural stem and progenitor cells. *Nanosci. Nanotechnol. Lett.* **2017**, *9*, 1491–1496.
- (4) Feng, X.; Han, T.; Xiong, Y.; Wang, S.; Dai, T.; Chen, J.; Zhang, X.; Wang, G. Plasmon-Enhanced Electrochemiluminescence of Silver Nanoclusters for microRNA Detection. *ACS Sens.* **2019**, *4*, 1633–1640.
- (5) Chen, J.; Han, T.; Feng, X.; Wang, B.; Guangfeng Wang, G. A poly(thymine)-templated fluorescent copper nanoparticle hydrogel-based visual and portable strategy for an organophosphorus pesticide assay. *Analyst* **2019**, *144*, 2423–2429.
- (6) Han, T.; Zhu, S.; Wang, S.; Wang, B.; Zhang, X.; Wang, G. Fluorometric methods for the determination of H₂O₂, glucose and cholesterol by using MnO₂ nanosheets modified with 5-carboxyfluorescein. *Microchim. Acta* **2019**, *186*, 269.
- (7) Daniel, M. C.; Astruc, D. Gold nanoparticles: assembly, supramolecular chemistry, quantum-size-related properties, and applications toward biology, catalysis, and nanotechnology. *Chem. Rev.* **2004**, *104*, 293–346.
- (8) Sosnik, A.; Carcaboso, M. A.; Glisoni, J. R.; Moretton, A. M.; Chiappetta, A. D. New novel challenges in tuberculosis: potentially effective nanotechnologies in drug delivery. *Adv. Drug Delivery Rev.* **2010**, *62*, 547–559.
- (9) Meng, F.; Cheng, R.; Deng, C.; Zhong, Z. Intracellular drug release nanosystems. *Mater. Today* **2012**, *15*, 436–442.
- (10) Medarova, Z.; Pham, W.; Farrar, C.; Petkova, V.; Moore, A. *In vivo* imaging of siRNA delivery and silencing in tumors. *Nat. Med.* **2007**, *13*, 372–377.
- (11) Li, Y. J.; Li, H. X.; Wang, F. L.; Kuang, X.; Hang, X. Z.; Deng, Y.; Du, R. J. Therapeutic efficacy of a novel non-peptide $\alpha\beta3$ integrin antagonist for pathological retinal angiogenesis in mice. *Exp. Eye Res.* **2014**, *129*, 119–126.
- (12) Movia, D.; Gerard, V.; Maguire, M. C.; Jain, N.; Bell, P. A.; Nicolosi, V.; O'Neill, T.; Scholz, D.; Gun'ko, Y.; Volkov, Y.; Prina-Mello, A. A safe-by-design approach to the development of gold nanoboxes as carriers for internalization into cancer cells. *Biomaterials* **2014**, *35*, 2543–2557.
- (13) Lin, Y. W.; Huang, C. C.; Chang, T. H. Gold nanoparticle probes for the detection of mercury, lead, and copper ions. *Analyst* **2011**, *136*, 863–871.
- (14) Dreaden, E. C.; Alkilany, M. A.; Huang, X.; Murphy, J. C.; El-Sayed, A. M. The golden age: gold nanoparticles for biomedicine. *Chem. Soc. Rev.* **2012**, *41*, 2740–2779.
- (15) Farooq, M. U.; Novosad, V.; Rozhkova, A. E.; Wali, H.; Ali, A.; Fateh, A. A.; Neogi, B. P.; Neogi, A.; Wang, Z. Gold nanoparticles-enabled efficient dual delivery of anticancer therapeutics to HeLa cells. *Sci. Rep.* **2018**, *8*, 1–12.
- (16) Gad, S. C.; Sharp, L. K.; Montgomery, C.; Payne, D. J.; Goodrich, P. G. Evaluation of the toxicity of intravenous delivery of auroshell particles (gold–silica nanoshells). *Int. J. Toxicol.* **2012**, *31*, 584–594.
- (17) Schwartz, J. A.; Shetty, M. A.; Price, E. R.; Stafford, J. R.; Wang, C. J.; Uthamanthil, K. R.; Pham, K.; McNichols, J. R.; Coleman, L. C.; Payne, D. J. Feasibility study of particle-assisted laser ablation of brain tumors in orthotopic canine model. *Cancer Res.* **2009**, *69*, 1659–1667.
- (18) Jana, N. R.; Gearheart, L.; Murphy, J. C. Seeding growth for size control of 5–40 nm diameter gold nanoparticles. *Langmuir* **2001**, *17*, 6782–6786.
- (19) Rao, C.; Müller, A.; Cheetham, K. A. *The Chemistry of Nanomaterials: Synthesis, Properties and Applications*; Wiley-VCH, 2004; p. 761.
- (20) Kumar, B.; Smita, K.; Cumbal, L.; Debut, A. Extracellular biofabrication of gold nanoparticles by using Lantana camara berry extract. *Inorg. Nano-Met. Chem.* **2017**, *47*, 138–142.
- (21) Fumiya, K.; Yugo, K.; Kazuo, F.; Toshihiro, K.; Yuki, I.; Etsuro, Y.; Suzuki, M. Formation of gold nanoparticles by glycolipids of *Lactobacillus casei*. *Sci. Rep.* **2016**, *6*, 34626.
- (22) Kumari, M.; Mishra, A.; Pandey, S.; Singh, P. S.; Chaudhry, V.; Mudiam, R. K. M.; Shukla, S.; Kakkar, P.; Nautiyal, S. C. Physico-chemical condition optimization during biosynthesis lead to the development of improved and catalytically efficient gold nanoparticles. *Sci. Rep.* **2016**, *6*, 27575.
- (23) Singh, S. K.; Singh, S.; Lillard, W. J., Jr.; Singh, R. Drug delivery approaches for breast cancer. *Int. J. Nanomed.* **2017**, *12*, 6205.
- (24) Salam, H. A.; Sivaraj, R.; Venckatesh, R. Green synthesis and characterization of zinc oxide nanoparticles from *Ocimum basilicum* L. var. *purpurascens* Benth.-Lamiaceae leaf extract. *Mater. Lett.* **2014**, *131*, 16–18.
- (25) Chandran, S. P.; Chaudhary, M.; Pasricha, R.; Ahmad, A.; Sastry, M. Synthesis of gold nanotriangles and silver nanoparticles using *Aloe vera* plant Extract. *Biotechnol. Prog.* **2006**, *22*, 577–583.
- (26) Talib, A.; Khan, M. S.; Gedda, G.; Wu, H. F. Stabilization of gold nanoparticles using natural plant gel: A greener step towards biological applications. *J. Mol. Liq.* **2016**, *220*, 463–467.
- (27) Philip, D. Honey mediated green synthesis of gold nanoparticles. *Spectrochim. Acta A* **2009**, *73*, 650–653.
- (28) Nakkala, J. R.; Mata, M.; Bhagat, E.; Sadras, S. R. Green synthesis of silver and gold nanoparticles from *Gymnema sylvestre* leaf extract: study of antioxidant and anticancer activities. *J. Nanopart. Res.* **2015**, *17*, 151–165.
- (29) Kumar, V.; Yadav, S. K. Plant-mediated synthesis of silver and gold nanoparticles and their applications. *J. Chem. Technol. Biotechnol.* **2009**, *84*, 151–157.
- (30) Liu, H.; Zhang, H.; Wang, J.; Wei, J. Effect of temperature on the size of biosynthesized silver nanoparticle: deep insight into microscopic kinetics analysis. *Arab. J. Chem.* **2020**, *13*, 1011–1019.
- (31) Yang, Z.; Li, Z.; Lu, X.; He, F.; Zhu, X.; Ma, Y.; He, R.; Gao, F.; Ni, W.; Yi, Y. Controllable biosynthesis and properties of gold nanoplates using yeast extract. *Nano-micro Lett.* **2017**, *9*, 5.
- (32) Huang, X.; El-Sayed, A. M. Gold nanoparticles: Optical properties and implementations in cancer diagnosis and photothermal therapy. *J. Adv. Res.* **2010**, *1*, 13–28.
- (33) Mayer, K. M.; Hafner, H. J. Localized surface plasmon resonance sensors. *Chem. Rev.* **2011**, *111*, 3828–3857.
- (34) Srinath, B.; Rai, R. V. Biosynthesis of highly monodispersed, spherical gold nanoparticles of size 4–10 nm from spent cultures of *Klebsiella pneumoniae*. *3 Biotech* **2015**, *5*, 671–676.
- (35) Zuber, A.; Purdey, M.; Schartner, E.; Forbes, C.; Van der Hoek, B.; Giles, D.; Abell, A.; Monro, T.; Ebendorff-Heidepriem, H. Detection of gold nanoparticles with different sizes using absorption and fluorescence-based method. *Sens. Actuators, B* **2016**, *227*, 117–127.
- (36) Alkilany, A. M.; Murphy, J. C. Toxicity and cellular uptake of gold nanoparticles: what we have learned so far? *J. Nanopart. Res.* **2010**, *12*, 2313–2333.
- (37) Mountrichas, G.; Pispas, S.; Kamitsos, I. E. Effect of temperature on the direct synthesis of gold nanoparticles mediated by poly (dimethylaminoethyl methacrylate) Homopolymer. *J. Phys. Chem. C* **2014**, *118*, 22754–22759.
- (38) Das, S. K.; Das, R. A.; Guha, A. K. Microbial synthesis of multi-shaped gold nanostructures. *Small* **2010**, *6*, 1012–1021.
- (39) Das, S. K.; Dickinson, C.; Lafir, F.; Brougham, F. D.; Marsili, E. Synthesis, characterization and catalytic activity of gold nanoparticles

biosynthesized with *Rhizopus oryzae* protein extract. *Green Chem.* **2012**, *14*, 1322–1334.

(40) Snitka, V.; Naumenko, D. O.; Ramanauskaite, L.; Kravchenko, S. A.; Snopok, B. A. Generation of diversiform gold nanostructures inspired by honey's components: Growth mechanism, characterization, and shape separation by the centrifugation-assisted sedimentation. *J. Colloid Interface Sci.* **2012**, *386*, 99–106.

(41) Ogundare, O. B.; Akinribide, O. J.; Adetunji, A. R.; Adeoye, M. O.; Olubambi, P. A. Crystallite size determination of thermally deposited Gold Nanoparticles. *Procedia Manuf.* **2019**, *30*, 173–179.

(42) Yu, X.; Lei, D. Y.; Amin, F.; Hartmann, R.; Acuna, G. P.; Guerrero-Martínez, A.; Maier, S. A.; Tinnefeld, P.; Carregal-Romero, S.; Parak, W. J. Distance control in-between plasmonic nanoparticles via biological and polymeric spacers. *Nano Today* **2013**, *8*, 480–493.

(43) McKeon, V. A. The breast cancer prevention trial: should women at risk take tamoxifen? *J. Obstet. Gynecol. Neonatal. Nurs.* **1999**, *28*, 34–38.

(44) Fisher, B.; Costantino, J. P.; Wickerham, D. L.; Redmond, C. K.; Kavanah, M.; Cronin, W. M.; Vogel, V.; Robidoux, A.; Dimitrov, N.; Atkins, J.; Daly, M. Tamoxifen for prevention of breast cancer: report of the National Surgical Adjuvant Breast and Bowel Project P-1 Study. *J. Natl. Cancer. Inst.* **1998**, *90*, 1371–1388.

(45) Radmacher, M. D.; Simon, R. Estimation of tamoxifen's efficacy for preventing the formation and growth of breast tumors. *J. Natl. Cancer. Inst.* **2000**, *92*, 48–53.

(46) Sakamoto, T.; Niiya, D.; Seiki, M. Targeting the Warburg effect that arises in tumor cells expressing membrane type-1 matrix metalloproteinase. *J. Biol. Chem.* **2011**, *286*, 14691–14704.

(47) Gatenby, R. A.; Gillies, R. J. Why do cancers have high aerobic glycolysis? *Nat. Rev. Cancer* **2004**, *4*, 891–899.

(48) Mostafavi, E.; Zarepour, A.; Barabadi, H.; Zarrabi, A.; Truong, L. B.; Medina-Cruz, D. Antineoplastic activity of biogenic silver and gold nanoparticles to combat leukemia: beginning a new era in cancer theragnostic. *Biotechnol. Rep.* **2022**, *34*, No. e00714.

(49) Sargazi, S.; Laraib, U.; Er, S.; Rahdar, A.; Hassanisaadi, M.; Zafar, M. N.; Bilal, M. Application of Green Gold Nanoparticles in Cancer Therapy and Diagnosis. *Nanomaterials* **2022**, *12*, 1102.

(50) Hosny, M.; Fawzy, M.; El-Badry, Y. A.; Hussein, E. E.; Eltaweil, A. S. Plant-assisted synthesis of gold nanoparticles for photocatalytic, anticancer, and antioxidant applications. *J. Saudi Chem. Soc.* **2022**, *26*, No. 101419.